Neuron, Vol. 44, 835–849, December 2, 2004, Copyright ©2004 by Cell Press

Enhancement of Synaptic Plasticity through Chronically Reduced Ca^{2+} Flux during Uncorrelated Activity

Inna Slutsky, Safa Sadeghpour, Bing Li, and Guosong Liu*
Department of Brain and Cognitive Sciences
Picower Center for Learning and Memory and
RIKEN-MIT Neuroscience Center
Massachusetts Institute of Technology
Cambridge, Massachusetts 02139

Summary

The plasticity of synapses within neural circuits is regulated by activity, but the underlying mechanisms remain elusive. Using the dye FM1-43 to directly image presynaptic function, we found that large numbers of presynaptic terminals in hippocampal cultures have a low release probability. While these terminals were not readily modifiable, a transient but not permanent long-term reduction of network activity or Ca^{2+} influx could increase their modifiability. This modulation of plasticity was mediated by Ca^{2+} flux through NMDA and voltage-gated calcium channels and was lost within 48 hr. A more permanent enhancement of synaptic plasticity was achieved by selectively reducing the Ca^{2+} flux associated with uncorrelated activity via adjustment of the voltage-dependent Mg^{2+} block of the NMDAR. Upregulation of NR2B-containing NMDARs induced by this treatment is an important but not sole contributor to the enhancement of plasticity. Thus, quantity and quality of activity have differential effects on the intrinsic plasticity of neurons.

Introduction

Synaptic plasticity is known to be essential for achieving the proper organization of neural circuits during early development and for the storage of information in later stages. However, the regulation of intrinsic plasticity of synapses under physiological conditions is not fully understood. Prior work on the regulation of cortical map plasticity during development provides important clues. Pioneering studies by Hubel and Wiesel (Weisel and Hubel, 1963) demonstrate that there exists a critical period during which depriving an eye of visual input dramatically alters thalamo-cortical projections in favor of the other eye. Since then, many other experiments have been carried out to determine the mechanisms that engender this critical period during which reorganization of cortical connections is possible (Stryker and Harris, 1986; Shatz and Stryker, 1988; reviewed in Katz and Shatz, 1996). We now know that, in the visual system, a developmental increase of neural input and activity leads to the eventual downregulation of the malleability of cortical representations. In contrast, reducing input activity via dark rearing prolongs the critical period for ocular dominance plasticity (Timney et al., 1978; Fagiolini et al., 1994). Similar relationships between activity and circuitry reorganization have since been established in somatosensory (Fox, 1992) and auditory (Chang and Merzenich, 2003) cortices as well. Thus, as a general trend, changes in ongoing neural activity correlate inversely with topographic map plasticity in these hierarchically early sensory cortices.

As the plasticity of individual synapses is essential for reorganization of cortical connections (reviewed in Buonomano and Merzenich, 1998; Bear, 2003), it is possible that the above relationship also holds between activity and synaptic plasticity. While it is well known that brief bursts of activity (seconds/minutes; $\sim 10^2$ action potentials [APs]) modify the efficacy of synaptic connections and their plasticity in neuronal circuits, the long-term effect of neural activity ($>$hours-lifetime; $\sim 10^3$–10^8 APs) on synaptic and cellular plasticity remains elusive (Abraham and Bear, 1996).

In this study, we first set out to determine the elementary relationship between the network's level of neural activity and the plasticity of its individual synapses. To achieve this goal, we needed to be able to modify neural activity and then directly monitor the plasticity of large numbers of synapses. To accomplish this, we employed a reduced experimental preparation of hippocampal neurons in culture where we could, in a clear-cut fashion, both control the activity and monitor the functional state and plasticity of large numbers of presynaptic terminals. We have used this system to answer these initial questions: Do neural activity and inhibition play a critical role in the plasticity of hippocampal synapses as they do in early sensory cortices? If so, is the magnitude of plasticity tuned continuously and reversibly according to the level of activity? What is the intermediary signaling pathway that relates the quantity/quality of activity to synaptic plasticity? For this last question, we wished to distinguish between membrane depolarization and Ca^{2+} flux as potential secondary messengers of importance and determine whether it is the integral (quantity) or precise spatiotemporal pattern (quality) of this intermediary that is the critical regulator. Finally, we explored the synaptic properties that might be essential for a synapse to be and remain plastic.

We found that the neural circuit contained large numbers of synaptic terminals with low probability of release, thus constituting a large reserve pool of "quiet" connections. The plasticity of these terminals was enhanced following the reduction of neural activity. We identified Ca^{2+} flux through NMDA and voltage-gated calcium channels (VGCCs) as the messenger that regulates the plasticity of synapses and release of BDNF as a mediator of presynaptic potentiation. However, we found that uniform reduction of Ca^{2+} flux failed to induce long-lasting enhancement of synaptic plasticity, suggesting a complex role for Ca^{2+} flux in the regulation of presynaptic plasticity. Interestingly, selective attenuation of NMDAR-mediated Ca^{2+} flux during uncorrelated activity obtained by adjusting the voltage-dependent Mg^{2+} blockade resulted in a permanent conversion of synapses to a plastic state. We deduce that the inverse and reversible relationship between the neural activity and synaptic

*Correspondence: liu@mit.edu

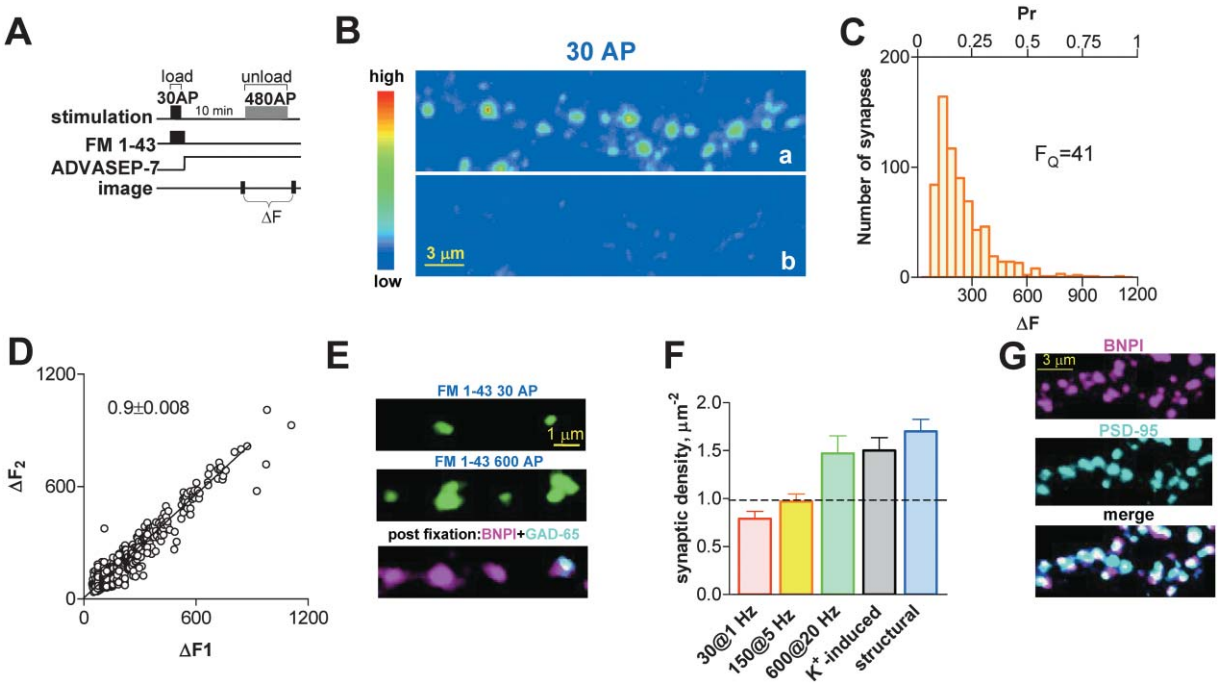

Figure 1. Distribution of Pr in Single Synapses of Hippocampal Networks

(A) Experimental protocol used to determine Pr of presynaptic terminals.

(B) Fluorescent images following loading with 30 AP (Ba) and unloading (Bb). Fluorescence intensities (arbitrary units) are coded using a pseudocolor transformation shown on the left side of the images.

(C) Distribution of ΔF obtained for 30 APs and converted to Pr, using the $F_Q = 41$ value as a conversion factor. The median of Pr is 0.14.

(D) Correlation between ΔF_1 and ΔF_2 obtained for two consequent loading-unloading protocols.

(E) Fluorescent images obtained following functional labeling with FM1-43 for 30 AP at 1 Hz and 600 AP at 20 Hz. Retrospective immunohistochemical staining of the same region revealed that only half of the boutons that were stained with VGLUT1 (for excitatory terminals) or GAD65 (for inhibitory terminals) correspond to FM-(+) terminals loaded by the 30 AP protocol.

(F) Comparison between structural and functional synaptic density at various conditions.

(G) Colocalization of the presynaptic marker VGLUT1 and the postsynaptic marker PSD-95.

plasticity, mediated through precise patterning of Ca^{2+} fluxes, may represent an elementary property of hippocampal circuits.

Results

The Majority of Presynaptic Terminals Exhibit a Low Probability of Release

To understand precisely the mechanisms regulating hippocampal synaptic plasticity, the physiological properties of individual synapses had to be studied. First, we determined the distribution of release probability (Pr) of single CNS synapses by counting the number of presynaptic vesicles turned over by a fixed number of action potentials using activity-dependent FM dye uptake as a marker (Ryan et al., 1996; Murthy et al., 1997; Murthy and Stevens, 1998). Action potentials triggered synaptic vesicle exocytosis and endocytosis, which labeled exocytosed vesicles with FM1-43 (see Figure 1A for loading protocol). Figure 1Ba shows an image containing several FM dye puncta following FM1-43 loading for 30 APs. The majority of FM dye spots were destained as a result of the second stimulation set (480 AP at 2 Hz, Figure 1Bb). We calculated the total amount of releasable fluorescence at each bouton (ΔF) from the difference between initial (Figure 1Ba) and final fluorescence (Figure 1Bb). From this value, we inferred the number of exocytosed synaptic vesicles per individual terminal by calculating the ratio $\Delta F/F_Q$, where F_Q is the estimated releasable fluorescence of a single synaptic vesicle. Thus, the Pr of individual terminals was calculated by $Pr = \Delta F/(N_{AP} \times F_Q)$, where N_{AP} is the number of APs applied during loading. If one can detect a ΔF as small as F_Q, this permits one to monitor terminals with extremely low Pr. We determined that F_Q is $\sim$40 in our imaging system (see Supplemental Figure S1 [http://www.neuron.org/cgi/content/full/44/5/835/DC1/]). This F_Q value was used to convert the ΔF histogram to a Pr distribution of individual synaptic terminals (Figure 1C). The Pr distribution has a skewed shape favoring low values (median = 0.14). Application of 30 APs under such conditions would ensure the detection of functional terminals with $Pr > 0.04$.

Since only those synaptic terminals with $Pr > 0.04$ were detected, we hypothesized that there must exist a population of terminals with lower Pr that were not being detected by this procedure. To determine both the number and the proportion of very low Pr terminals to total functional synaptic terminals, we compared the colocalization of FM puncta obtained from the 30 AP loading with puncta obtained using fluorescent antibodies against specific presynaptic proteins. VGLUT1 and

GAD65 antibodies were used to mark glutamatergic and GABAergic terminals, respectively. After FM images were obtained, the specimens were rapidly fixed and stained with antibodies (see Experimental Procedures). The two sets of images were aligned, allowing comparisons of functional terminals with their structural equivalents (Figure 1E). Most FM puncta were colocalized with spots labeled by antibodies against presynaptic proteins (Ryan et al., 1993; Schikorski and Stevens, 2001). To ensure that these functional presynaptic boutons were part of functional synapses, composed of both pre- and postsynaptic machinery, we examined whether spots labeled by VGLUT1 antibody were colocalized with those marked by PSD-95 antibody, a critical protein present in the postsynaptic spine of glutamatergic synapses. All VGLUT1 spots were colocalized with PSD-95 spots (Figure 1G). Thus, the majority of FM dye uptake occurred specifically within structurally complete synaptic terminals. However, not all synaptic terminals took up FM dye after 30 APs (Figure 1E). In fact, only 46% of structural synapses were stained during the 30 AP stimulation/loading protocol (Figures 1E and 1F). To determine the functional status of these seemingly nonfunctional terminals, we increased the technique's sensitivity by increasing the number of APs to 150 and the frequency of stimulation to 5 Hz. This protocol facilitates the release of vesicles from low Pr synapses without causing extensive depression of high Pr synapses (Murthy et al., 1997). Twenty percent more functional synapses were detected by this procedure, which is consistent with a previous report (Murthy et al., 1997). To determine whether the remaining 30% of synapses were capable of having vesicle turnover at all, we applied a maximal stimulation protocol (600 AP at 20 Hz). Compared with labeling under the 30 AP protocol in the same region, the number of FM-positive puncta that correlated with structurally identified synapses doubled to 88%.

We have interpreted the lack of FM uptake after 30 action potentials as meaning that the terminals have too low a Pr to exocytose their vesicles even after such a sequence of depolarizing events. An alternative possibility is a potential failure of action potentials to reach synaptic terminals. We considered this unlikely for the following reasons. (1) Synaptic failure in hippocampal slices could not be attributed to the failure of action potential propagation to synaptic terminals at the low stimulation frequency (Allen and Stevens, 1994; Raastad and Shepherd, 2003). (2) It has been demonstrated previously that Ca^{2+} flux in synaptic terminals is reliably generated in cultured hippocampal preparation (Ryan and Smith, 1995; Mackenzie et al., 1996). (3) The numbers of FM-positive puncta detected after maximal electrical stimulation (600 AP at 20 Hz) were similar to those obtained by 50 mM K^+ stimulation (Figure 1F), a method that depolarizes all terminals directly by generating prolonged opening of Ca^{2+} channels (Betz et al., 1992; Ryan et al., 1993). (4) In the presence of 100 ng/ml of neurotrophin BDNF, which is known to increase the Pr of synaptic terminals without changing their electrical excitability (Li et al., 1998), we found that all structural synaptic terminals became capable of taking up FM dye with the 30 AP protocol (see Figure 3B).

In summary, our results show that most synapses had a relatively low Pr (median = 0.14) and that roughly 50% of all structural synapses had a Pr $<$ 0.04.

Synapses with Low Probability of Release Are Not Potentiated by Theta Burst Stimulation

Given the inverse relationship between the initial strength and plasticity of a synapse (Bi and Poo, 1998), these low Pr terminals should in theory be highly potentiable. To test this possibility, we employed a plasticity induction method that is believed to replicate neural activity in vivo—theta burst stimulation (TBS) (Bliss and Collingridge, 1993). The induction-associated changes in Pr of synaptic terminals were determined by comparing ΔF_1 and ΔF_2, before and 30 min after TBS (30 bursts, each containing 5 APs at 25 Hz, 500 ms interburst interval). Surprisingly, no potentiation of Pr, indexed through significant changes in FM dye loading, was observed following the theta burst induction protocol (Figures 2Aa–2Ac). No changes were found either in the distribution of release probabilities (Figure 2C) or in the slope of $\Delta F_2/\Delta F_1$ (Figure 2F, blue circles). On average, $\Delta F_2/\Delta F_1$ (the ratio of fluorescence signal per FM spot) was 0.9 $\pm$ 0.2 and N_2/N_1 (the ratio of the number of detectable FM-positive terminals) was 1.2 $\pm$ 0.2 (Figure 1H). We also employed F $\times$ N to represent the total synaptic strength (S) within a given region of the hippocampal network. There were no significant differences in S_2/S_1 (1.1 $\pm$ 0.4, n = 8432, N=13 [where n is the number of terminals and N is the number of experiments], p = 0.15). This lack of potentiation was also observed 10 min following the induction protocol, also suggesting a lack of short-term potentiation (n = 3671, N = 5, p = 0.3). To confirm that the applied induction protocol was sufficient to reach the LTP threshold (Bear, 2003), we quadrupled the total number of action potentials used for TBS induction (600 AP). Still, no detectable changes of synaptic strength were found (S_2/S_1 = 1.2 $\pm$ 0.4, n = 3903, N = 4). These data suggest that low Pr synaptic terminals are not by default potentiable with TBS, leading us to ask what conditions would make such synapses plastic.

Reduction of Neuronal Activity Triggers Enhancement of Synaptic Plasticity

Since the increase in neural activity during the maturation of neural circuitry is associated with a reduction in the plasticity of synapses, we hypothesized that the level of neural activity in networks might directly influence the plasticity of synapses. If so, a reduction of neural activity would help convert nonplastic synapses into plastic ones. To test this possibility, we pretreated culture neurons for 4 hr with 100 nM TTX, a concentration blocking 95% of neuronal activity (Figure 4D). Using the induction protocol described above, we tested the plasticity of presynaptic terminals in the TTX-treated cultures (Figure 2B; the treatment drug was not present during induction protocol). In this case, there was an increase in FM dye loading after TBS and thus measured Pr of the synaptic terminals, although the initial Pr of synapses did not change significantly (Figures 2Ad–2Af). Quantitatively, there were two distinct changes in FM1-43 staining properties after TBS-mediated induction: (1) an increase in the fluorescence intensity of puncta detected in the basal condition, indicating an increase in the average

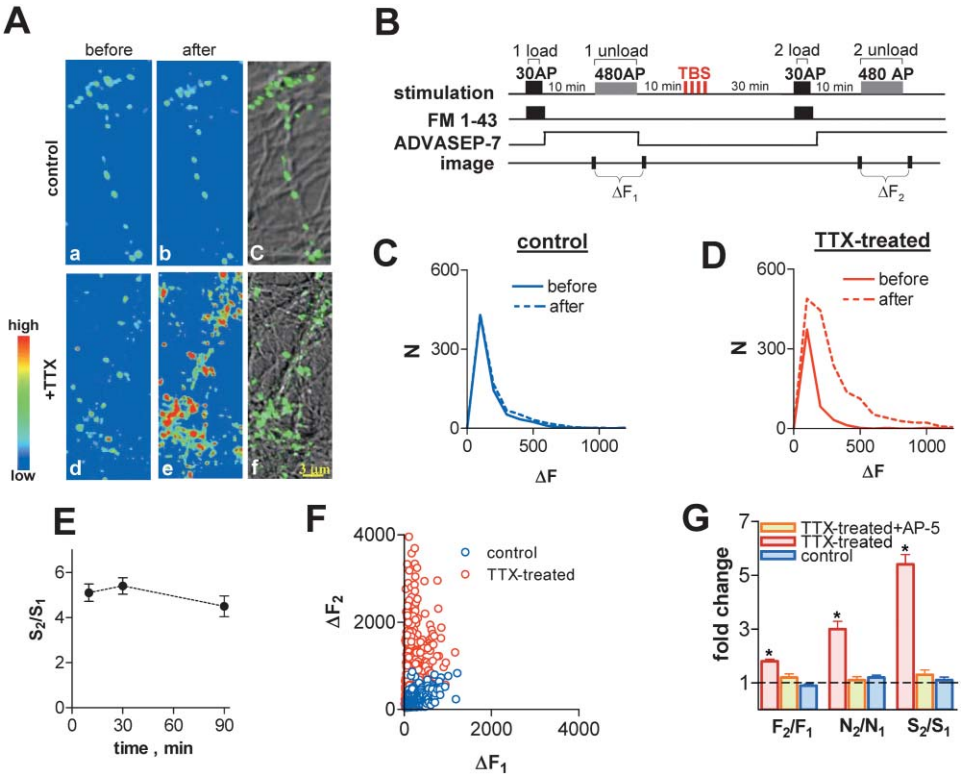

Figure 2. Reduction of Neural Activity Induces Enhancement of Synaptic Plasticity

(A) Representative fluorescent images, before and 30 min after TBS in control (Aa and Ab) and TTX-treated (100 nM, 6 hr) (Ad and Ae) cultures. DIC images of the same regions (Ac and Af). Fluorescence intensities (arbitrary units) are coded using a pseudocolor transformation shown to the left of the images.

(B) Experimental protocol designed to determine ΔF of synapses before and after plasticity induction. TBS (30 bursts, each containing 5 AP at 25 Hz, 500 ms interburst interval) used as induction protocol.

(C) Histograms of ΔF of 704 boutons in control cultures before (solid lines) and after (dotted lines) TBS from the images shown in (Aa) and (Ab). There is no change in ΔF distribution in control cultures.

(D) Histograms of ΔF of 508 boutons in TTX-treated cultures before (solid lines) and after (dotted lines) TBS from the images shown in (Ad) and (Ae). ΔF median increased from 100 to 213, and the number of FM-detectable boutons increased from 508 to 1608.

(E) Plasticity enhancement lasts at least 1.5 hr after TBS induction.

(F) Correlation between ΔF of active boutons before and after TBS in control ($N = 6$, blue circles) and TTX-treated ($N = 5$, red circles) cultures.

(G) Average magnitude of plasticity (S_2/S_1) for different groups of cultures: 1.1 ± 0.1 for control ($N = 13$), 5.4 ± 0.4 for TTX-treated ($N = 7$), and 1.3 ± 0.2, for TTX-treated in the presence of 50 μM AP-5 during TBS ($N = 5$).

Pr; and (2) an increase in the total number of detected FM-positive boutons, indicating a conversion of terminals with a Pr < 0.04 (undetectable) to a state of Pr > 0.04. Since this phenomenon was observable 10 min after TBS, we concluded that synaptogenesis was unlikely. For the experiment depicted in Figures 2Ad and 2Ae, the median value of ΔF_2 increased 2-fold after the TBS protocol, while the number of detectable fluorescent spots increased from 508 to 1608 (Figure 2D). The collective results of these experiments ($n = 4328$, $N = 7$) are shown in Figure 2G. After TBS, the probability of release, on average, increased 1.8-fold ($p < 0.001$), accompanied by a simultaneous 3-fold increase in FM-positive synaptic density ($p < 0.001$). Total presynaptic strength (S) increased 5.4-fold after induction in the TTX-treated cultures (red bars). This potentiation was also long lasting: a stable increase in synaptic strength was detected from 10 min to 1.5 hr after TBS (Figure 2E). We refer to this presynaptic potentiation as "plasticity" throughout the rest of the paper. Thus, a reduction of AP generation through TTX-mediated blockade of Na^+ channels can induce an enhancement of synaptic plasticity.

Since it is known that the activation of NMDARs during TBS is essential for the induction of synaptic plasticity, we tested whether a TBS-induced increase of Pr required NMDAR activation. No detectable changes in ΔF were observed if the NMDAR blocker AP-5 (50 μM) was present during theta burst delivery ($n = 4207$, $N = 5$, $p = 0.2$, Figure 2G, yellow bars), indicating the necessity of NMDARs for inducing this type of synaptic plasticity.

BDNF Release Is Necessary for TBS-Induced Presynaptic Potentiation

We further characterized the signal involved in relating TBS to presynaptic potentiation. Recent studies have indicated that the release of BDNF is required in the expression of the presynaptic component of theta burst-induced potentiation in hippocampal CA3-CA1 synapses (Kang et al., 1997; Zakharenko et al., 2003). We

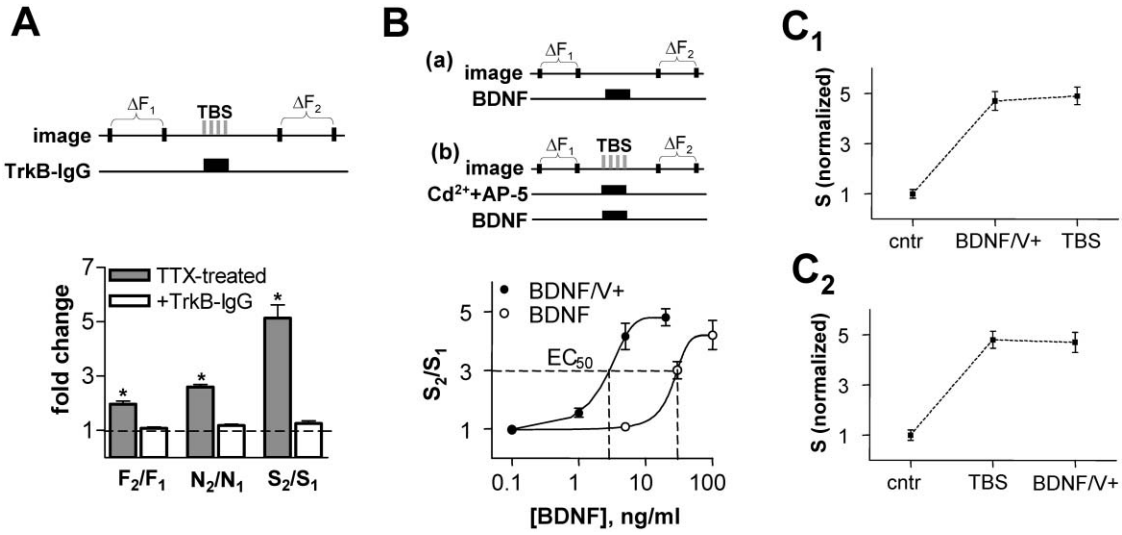

Figure 3. BDNF as a Mediator of TBS-Induced Presynaptic Potentiation

(A) TrkB-IgG (4 μg/ml), applied during TBS, significantly decreases the magnitude of presynaptic potentiation, compared to TTX-treated sister cultures. S_2/S_1 for treated cultures is 5.1 ± 0.5 (N = 4), and for treated cultures in the presence of TrkB-IgG, S_2/S_1 is 1.3 ± 0.1 (N = 5). (B) Dose response of Pr to exogenously applied BDNF: (Ba) BDNF alone (empty circles); (Bb) BDNF combined with TBS (filled circles) in the presence of cadmium (50 μM) and AP-5 (50 μM) to block pre- and postsynaptic Ca^{2+}-dependent BDNF release in plastic cultures (TTX-treated). EC_{50} for BDNF alone is 25 ng/ml, for BDNF combined with TBS, it is 2.4 ng/ml. (C_1) Application of BDNF 10 min before TBS occludes TBS-induced potentiation (N = 3, $p > 0.3$). (C_2) TBS applied 10 min before BDNF occludes the BDNF effect (N = 3, $p > 0.7$) in TTX-treated cultures. In both cases, BDNF was applied at 20 ng/ml.

used an extracellular TrkB-IgG fusion protein that chelates endogenously released TrkB ligands to block this putative pathway (Shelton et al., 1995). Application of TrkB-IgG (4 μg/ml) to hippocampal cultures 5 min prior to induction protocol (TBS) blocked TBS-induced presynaptic potentiation (S_2/S_1 = 5.1 ± 0.5, n = 3896, N = 4 in control group; S_2/S_1 = 1.3 ± 0.1, n = 4407, N = 5 with TrkB-IgG; Figure 3A). The presence of TrkB-IgG did not alter the properties of the presynaptic terminals under the basal condition or alter synaptic NMDA currents measured by double-patch recording (data not shown), confirming that endogenously released BDNF is necessary for the induction of presynaptic plasticity.

To confirm the role of BDNF in presynaptic potentiation, we studied the effects of exogenous application (3 min) of BDNF on the Pr of presynaptic terminals. Consistent with previous findings (Li et al., 1998), the Pr of presynaptic terminals can be upregulated directly by application of BDNF (EC_{50} = 25 ng/ml) (Figure 3B). Given the variety of cellular pathways that BDNF stimulates (Lu, 2003), we wished to use the lowest possible concentration to avoid the wide range of possible nonspecific effects. For this purpose, we examined whether the presynaptic efficacy of BDNF would be higher when the neuronal membrane was depolarized, as has been shown previously in the developing NMJ (Boulanger and Poo, 1999). We used TBS to depolarize while applying cadmium and AP-5 (both at 50 μM), blockers of VGCC and NMDA channels, respectively, to prevent Ca^{2+}-dependent release of endogenous BDNF. Under this condition (referred to as V+), there was no presynaptic potentiation (Figure 3B; leftmost point). When BDNF application was coupled with depolarization (V+), BDNF's efficacy was enhanced 10-fold (EC_{50} = 2.4 ng/ml, Figure 3B).

To determine whether BDNF/V+ and TBS-induced potentiation share the same pathway, we performed an occlusion experiment. Acute BDNF/V+ applied at a saturating concentration (20 ng/ml) occluded potentiation by TBS (Figure 3C_1), and BDNF/V+ failed to induce further potentiation after TBS (Figure 3C_2). Given the mutual occlusion, these data suggest that BDNF is an endogenous messenger for TBS-induced presynaptic potentiation.

Enhancement of Synaptic Plasticity Is Induced by Reduction of Ca^{2+} Flux

Given that the rate of neural firing is largely dependent on the concurrent balance of excitation and inhibition, shifting this balance may be a physiological way of altering the overall level of neuronal activity (Liu, 2004) (Figure 4A). If so, enhancement of inhibition or decrease of excitation should be as effective in enhancing synaptic plasticity as blocking TTX-sensitive Na^+ channels. Flunitrazepam was used to prolong $GABA_A$ receptor opening time and enhance the strength of GABAergic transmission (5 μM, 4–6 hr). The AMPA receptor (AMPAR) antagonist NBQX was used to decrease the strength of glutamatergic transmission (1 μM, 4–6 hr). Both treatments enhanced the plasticity of synapses. The probability of release, the number of FM-positive puncta, and the total presynaptic strength all increased after induction ($\Delta F_2/\Delta F_1$ = 1.5 ± 0.1, N_2/N_1 = 2.5 ± 0.2; S_2/S_1 = 3.8; n = 3107, N = 4; Figure 4B) in flunitrazepam-treated cultures. Similar results were found for NBQX-treated cultures ($\Delta F_2/\Delta F_1$ = 1.4 ± 0.1, N_2/N_1 = 2.1 ± 0.1; S_2/S_1 = 3.0; n = 2709, N = 4). Thus one can infer that a general reduction in activity, brought about by any of these means, is sufficient to induce potentiability in presynaptic terminals.

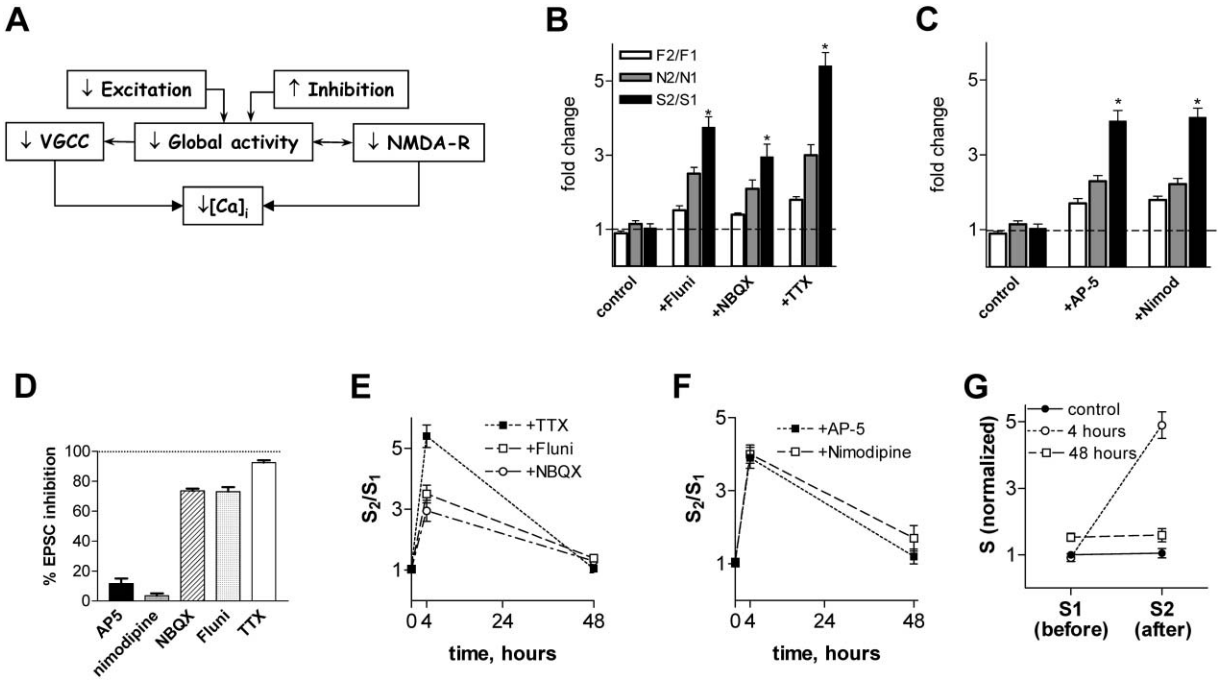

Figure 4. Enhancement of Plasticity of Synaptic Terminals by Shifting of Excitation-Inhibition Balance or Reduction in Ca^{2+} Flux

(A) Possible pathways to reduce Ca^{2+} flux in a postsynaptic cell.

(B) Enhancing postsynaptic inhibition by 4–6 hr treatment with flunitrazepam (5 μM) or reducing excitation by NBQX (1 μM) induces the upregulation of synaptic plasticity. S_2/S_1 is 3.8 ± 0.3 (N = 4) and 3.0 ± 0.3 (N = 4) for flunitrazepam and NBQX, respectively, compared to 5.4 ± 0.4 (N = 7) for TTX treatment.

(C) Short-term (4–6 hr) blockade of NMDAR or L-type VGCC induces enhancement of the plasticity of presynaptic terminals. Average results of treatment with AP-5 (20 μM) and nimodipine (10 μM) for the magnitude of synaptic plasticity: S_2/S_1 is 3.9 ± 0.3 (N = 4) and 4.0 ± 0.5 (N = 4) for AP-5 and nimodipine, respectively.

(D) Effects of AP-5 (20 μM), nimodipine (10 μM), NBQX (1 μM), flunitrazepam (5 μM), and TTX (100 nM) on neuronal activity, expressed as an integral of EPSCs at −60 mV.

(E) Synaptic terminals lose plasticity after prolonged reduction of neural activity with TTX (N = 5), NBQX (N = 5), and flunitrazepam (N = 8).

(F) Chronic incubation for 48 hr with AP-5 (N = 6) and nimodipine (N = 4) does not trigger an increase of synaptic plasticity.

(G) Comparison of presynaptic strength before (S_1) and after (S_2) TBS in control and 4 and 48 hr TTX-treated cultures. Short-term (4 hr) application of TTX did not significantly change initial presynaptic strength (S_1) ($p > 0.5$, N = 5). Long-term (48 hr) incubation induced 1.5 (±0.1)-fold increase in S_1 ($p < 0.005$, N = 6), which is significantly lower than the maximal TBS-induced potentiation (S_2 = 4.9 ± 0.4, N = 6). S values were normalized by S_1 of control cultures.

What intracellular mechanisms translate neural activity into modifications of synaptic plasticity? One natural candidate is Ca^{2+} flux through both NMDARs and VGCCs. The opening of both channels correlates strongly with global activity. Thus, we tested whether a reduction in Ca^{2+} flux was sufficient to enhance the plasticity of presynaptic terminals. Ca^{2+} influx to postsynaptic neurons is largely controlled by the opening of NMDARs during synaptic transmission or via the opening of L-type VGCC during action potentials. Thus, we tested the effects of chronic reduction of NMDAR activity or L-type VGCC opening on the plasticity of synaptic terminals. The block of NMDARs by 20 μM AP-5 (n = 2803, N = 2) or that of L-type VGCC by 10 μM nimodipine (n = 3321, N = 3) enhanced the plasticity of synaptic terminals (Figure 4C). Since these treatments, particularly nimodipine, did not affect the level of neural activity significantly (Figure 4D), we conclude that the reduction in Ca^{2+} flux was sufficient in itself to induce upregulation of synaptic plasticity.

Since we found that a transient reduction of neuronal activity for 4–6 hr increases the plasticity of the network, we asked whether a long-lasting reduction of neuronal activity, over a period of days, would generate similar results. To answer this question, we compared the degrees of synaptic plasticity after 4 and 48 hr of drug treatment, respectively. Surprisingly, after 48 hr of incubation, there was no significant TBS-induced potentiation whether the drug inhibited global activity (TTX, NBQX, flunitrazepam, Figure 4E) or decreased Ca^{2+} flux (AP-5, nimodipine, Figure 4F). In both cases, the neurons appeared healthy. One possibility is that, due to homeostatic mechanisms (reviewed in Turrigiano and Nelson, 2004), chronic inactivation led to a saturating increase of presynaptic efficacy (Bacci et al., 2001; Murthy et al., 2001; Thiagarajan et al., 2002), which in itself made them incapable of being further potentiated. Indeed, we found that Pr increased by 50% after 48 hr of activity blockade (Figure 4G). However, the TBS-induced potentiation in the short-term treated cultures was over 400% (Figure 4G). Despite the modest increase of Pr, these synapses had ample dynamic range to be potentiated. We can infer that the lack of plasticity during long-term reduction of Ca^{2+} flux is likely to be caused by other mechanisms.

Temporal Patterns of NMDA-Mediated Ca^{2+} Flux Can Be Modified by $[Mg^{2+}]_o$

It is puzzling that enhancements of plasticity were observable only if global reductions of neural activity or Ca^{2+} flux were restricted in time. Long-term reduction of neural activity must induce other biological changes that reduce the potentiability of synapses. Chronic perturbations of neural activity and calcium flux may disrupt normal function, leading to unexpected side effects. How, then, could the system induce physiologically relevant long-term enhancements of network potentiability? Since neither reducing global activity (through TTX, NBQX, or flunitrazepam) nor Ca^{2+} flux (through blockade of just VGCC channels or partial blockade of NMDA receptors) was effective in long-term treatments (Figure 4), we wished to examine whether selective reduction of different aspects of the network's patterns of Ca^{2+} flux would be capable of generating long-term potentiability.

In functional neural networks, the synaptic inputs induced by physiological stimuli tend to be correlated, while inputs from spontaneous activity of neural connections are uncorrelated (Lisman, 1997) (Figure 4A). The spatial and temporal structures of synaptic inputs are decoded into Ca^{2+} fluxes in postsynaptic neurons through the opening of NMDARs. By disturbing Ca^{2+} flux associated with one type of input and not the other, one might test the effects of various aspects of the patterns of Ca^{2+} flux on the synapses' potentiability. In that respect, the voltage-dependent effects of Mg^{2+} on NMDA channels were ideal for testing our hypothesis (Mayer et al., 1984; Nowak et al., 1984). Since the effects of Mg^{2+} block are strongest at resting potentials, the extracellular concentration of Mg^{2+} ($[Mg^{2+}]_o$) influences Ca^{2+} flux during uncorrelated synaptic inputs. By contrast, during depolarization, the magnesium block is removed completely. Thus, an elevation of $[Mg^{2+}]_o$ increases the blockade of NMDA channels during hyperpolarization, selectively reducing Ca^{2+} flux associated with uncorrelated activity while leaving depolarization-associated Ca^{2+} flux relatively unperturbed.

Although the biophysics of Mg^{2+} block have been studied extensively (Mayer et al., 1984; Nowak et al., 1984; Jahr and Stevens, 1990), we wished to determine precisely the behavior of the Mg^{2+} block at near-physiological concentrations. For example, while the original studies looked at a range from 0.5 to 10 mM of Mg^{2+}, this mineral is found in rodent cerebrospinal fluid (CSF) at a concentration of around 0.8 mM (Chutkow, 1974), and in humans, CSF $[Mg^{2+}]_o$ fluctuates between 1.0 and 1.2 mM (Kapaki et al., 1989). We evoked NMDA currents by iontophoretic application of glutamate to a putative single bouton identified by FM1-43 labeling and recorded under whole-cell patch clamp in the presence of the AMPAR blocker NBQX (10 μM). The glutamate delivered by this technique can be focal and rapid (Murnick et al., 2002), with the NMDA currents' time course roughly comparable to that of $EPSC_{NMDA}$ generated by presynaptically evoked release (Renger et al., 2001). When $[Mg^{2+}]_o$ was raised from 0.8 to 1.2 mM, it caused a 50% reduction of $EPSC_{NMDA}$ amplitude at -50 mV, while the size of the outward $EPSC_{NMDA}$ at $+40$ mV remained relatively unchanged. Further increases in $[Mg^{2+}]_o$ beyond 1.2 mM had significantly less effect on current.

To quantify this effect, we converted our measured NMDA currents into conductance (g) (Figure 4C). The voltage dependency of the Mg block did not vary significantly with increases in $[Mg^{2+}]_o$. However, apparent affinity, K_{Mg}, changed dramatically when $[Mg^{2+}]_o$ increased from 0.8 to 1.2 mM (Figure 5C and Table 1, see Experimental Procedures). Thus, within the known physiological range of CSF $[Mg^{2+}]_o$, small variations in $[Mg^{2+}]_o$ have profound influences on the affinity of Mg^{2+} for NMDAR. This region of high magnesium sensitivity could be used to selectively change the NMDAR-mediated Ca^{2+} flux near resting membrane potentials. To illustrate this effect quantitatively, we plotted the ratio of NMDA current amplitudes as a function of membrane potential at 0.8 and 1.2 mM $[Mg^{2+}]_o$ (Figure 5D). An increase in $[Mg^{2+}]_o$ from 0.8 to 1.2 mM led to an $\sim$60% reduction of NMDA current when the membrane potential was below -50 mV, but had no effect at depolarized potentials.

It is known that NMDA channels are highly Ca^{2+} permeable ($P_{Ca}/P_{Na} \sim 10$) (Mayer and Westbrook, 1987; Jahr and Stevens, 1993) and that Ca^{2+} influx through NMDARs accounts for most of synaptic spine Ca^{2+} (Yuste and Denk, 1995; Kovalchuk et al., 2000; Sabatini et al., 2002). In particular, since an elegant recent study by Sabatini et al. (2002) has shown that the time course of Ca^{2+} influx during NMDARs opening matches exactly with the temporal profile of Ca^{2+} life span in the spine, measured NMDAR currents can be used to predict the size of the Ca^{2+} flux. However, since our conclusions rest on the effects that perturbation of Ca^{2+} flux has on synaptic plasticity, we wished to directly confirm that changes of Mg^{2+} concentration cause a proportional change in NMDA-mediated $[Ca^{2+}]$ transients at single spines. Individual spines were visualized by filling the cell with both a fluorescent Ca^{2+} indicator dye (Fluo-5F) and Ca^{2+}-insensitive Alexa 633 (Sabatini et al., 2002) (Figure 5E). NMDARs at a single spine were activated by local iontophoresis of glutamate while the resulting NMDA currents and $[Ca^{2+}]$ transients were being monitored (Figure 5F). Consistent with the studies mentioned above, we observed that the amplitudes of synaptic NMDA currents and of $[Ca^{2+}]$ transients at the spine were linearly correlated ($r^2 = 0.99$, Figure 5G). Finally, to test whether Ca^{2+} flux had a similar sensitivity to $[Mg^{2+}]_o$ as NMDA currents, we compared the $[Ca^{2+}]$ transients and the NMDA currents at the same spines before and after an acute increase of $[Mg^{2+}]_o$. The amplitude of Ca^{2+} signal ($\Delta F/F$) and the amplitude of $EPSC_{NMDA}$ were reduced by 57% $\pm$ 5% and 54% $\pm$ 7%, respectively ($N = 3$, $p > 0.3$). Thus, the NMDA-mediated currents and Ca^{2+} flux are sensitive to physiological variations of $[Mg^{2+}]_o$.

As a control, we determined that raising $[Mg^{2+}]_o$ from 0.8 to 1.2 mM did not alter resting membrane potential (74 $\pm$ 1 mV at 0.8 mM; 73 $\pm$ 1 mV at 1.2 mM, $N = 5$), nor overall synaptic inputs during network activity ($EPSC_{1.2}/EPSC_{0.8} = 1.03 \pm 0.1$, $N = 5$). Furthermore, there were no detectable changes in amplitude and frequency of spontaneous miniature $EPSP_{AMPA}$s ($EPSP_{1.2}/EPSP_{0.8} = 0.9 \pm 0.1$, $N = 5$). The lack of detectable influence on the excitability of neurons and synaptic inputs during network activity can be explained by the relatively small increase in $[Mg^{2+}]_o$, which is insufficient to significantly alter the excitability of the membrane or the probability of transmitter release.

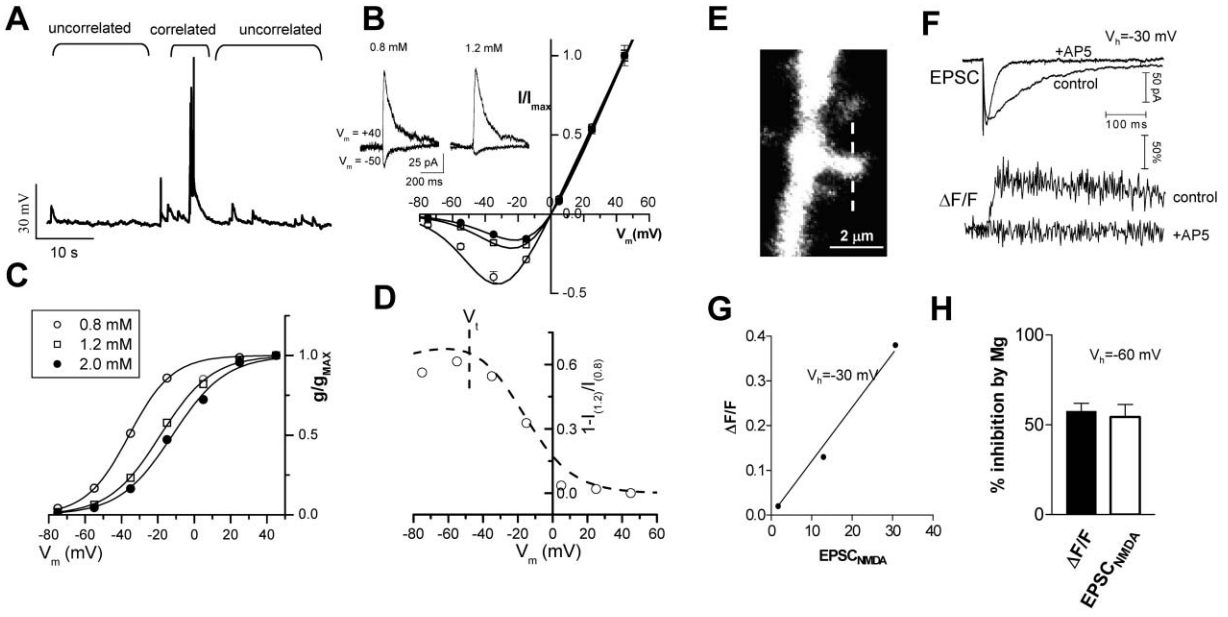

Figure 5. Voltage-Dependent NMDA Channel Opening Is Sensitive to Physiological Variation in $[Mg^{2+}]_o$

(A) Exemplary membrane potential trace recorded under current clamp showing uncorrelated (background) and correlated (bursting) patterns of neuronal activity.

(B) Normalized peak glutamate-activated NMDA currents plotted against membrane potential in three $[Mg^{2+}]_o$ (0.8, ○; 1.2, □; and 2.0 mM, ●). Membrane potentials were varied from −70 to +50 mV in 20 mV increments, and currents were recorded from cultured CA1 pyramidal neurons (N = 5). Since the evoked NMDA currents varied among the synapses examined, the amplitudes of NMDA currents were normalized to their maximum values to group all data points together.

(C) Normalized g-V relationship, where g/g_{max} was the peak conductance of NMDA channel at 0.8 (○), 1.2 (□), and 2 mM (●) $[Mg^{2+}]_o$. The continuous lines through points were obtained by fitting the g-V relationship with Equation 1 with the parameters δ and K_{Mg}.

(D) The fraction of NMDAR Mg^{2+} block at 1.2 mM $[Mg^{2+}]_o$ relating to 0.8 $[Mg^{2+}]_o$ as a function of membrane potential. Note the ~60% greater attenuation of NMDA current at the subthreshold range of membrane potential with 1.2 mM $[Mg^{2+}]_o$ and the decline of this effect when membrane potential crosses the threshold for action potential generation (marked as V_t).

(E) Dendritic spine visualized with Alexa 633.

(F) The time course of NMDA currents and associated Ca^{2+}-dependent fluorescence transients (ΔF/F, n = 3) in controls and following application of AP-5 (50 μM) from the spine depicted in (E).

(G) The amplitude of NMDA currents and Ca^{2+} influx (ΔF/F) at a single spine are linearly correlated ($r^2 = 0.99$).

(H) Elevation of $[Mg^{2+}]_o$ from 0.8 mM to 1.2 mM led to a parallel reduction of NMDA currents (57% ± 5%) and Ca^{2+} influx (54% ± 7%) (n = 3, Vm = −60 mV).

Elevation of $[Mg^{2+}]_o$ Triggers Formation of Highly Plastic Synapses

We cultured hippocampal neurons with both "normal" and "elevated" concentrations of $[Mg^{2+}]_o$ (control, 0.8 mM; experimental, 1.2 mM; 2 weeks). Neurons growing under the higher level of $[Mg^{2+}]_o$ had normal neuronal density and morphology. Unlike the control neurons, however, their synapses were highly plastic even after long-term treatment. Figure 6A provides representative images of presynaptic terminals before and 30 min after TBS in high Mg^{2+}-treated cultures. There are dramatic, sustained increases in FM1-43 staining after TBS stimulation (Figure 6A). The Pr increased 2.3-fold (±0.1, $p < 0.001$), and the number of detectable FM puncta increased 2.1-fold (±0.1, $p < 0.001$), resulting in a 5.5-fold increase in total presynaptic strength (n = 10618, N = 15, $p < 0.0001$, Figure 6B). This potentiation was stable for at least 1.5 hr (data not shown). This form of plasticity required NMDAR activation (50 μM AP-5 blocked induction; $S_2/S_1 = 1.1 \pm 0.2$, n = 3691, N = 5). In contrast to uniform reductions of Ca^{2+} flux (Figure 4F), synapses retained their plasticity even when $[Mg^{2+}]_o$ was elevated for several weeks.

Table 1. Woodhull Parameters for Voltage Dependency of Mg^{2+} Block as a Function of $[Mg^{2+}]_o$

$[Mg^{2+}]_o$ (mM)	K_{Mg} (mM)	δ	n
0.8	16.3 ± 1.0	1.00 ± 0.02	5
1.2	4.5 ± 0.3	0.90 ± 0.03	5
2.0	4.5 ± 0.4	0.87 ± 0.06	5

We attributed this effect to the selective influence of Mg^{2+} on Ca^{2+} flux associated with uncorrelated activity. However, the lack of long-lasting enhancement of plasticity with AP5-mediated blocking of NMDA channels (Figure 4F) may be due to the *complete* blockade of NMDA-mediated Ca^{2+} flux by AP-5. To determine whether this is the case, we repeated the experiment with a concentration of AP-5 (5 μM; IC_{50}) that matched the degree of Ca^{2+} flux reduction obtained via an increase in $[Mg^{2+}]_o$. The magnitude of presynaptic plasticity was tested in cultures following 4 hr, 48 hr, 2 weeks, and 3 weeks of incubation with either 5 μM AP-5, 20 μM AP-5, or 1.2 mM $[Mg^{2+}]_o$. The response to 4 hr reduction of Ca^{2+} flux was very similar across all treatments. The

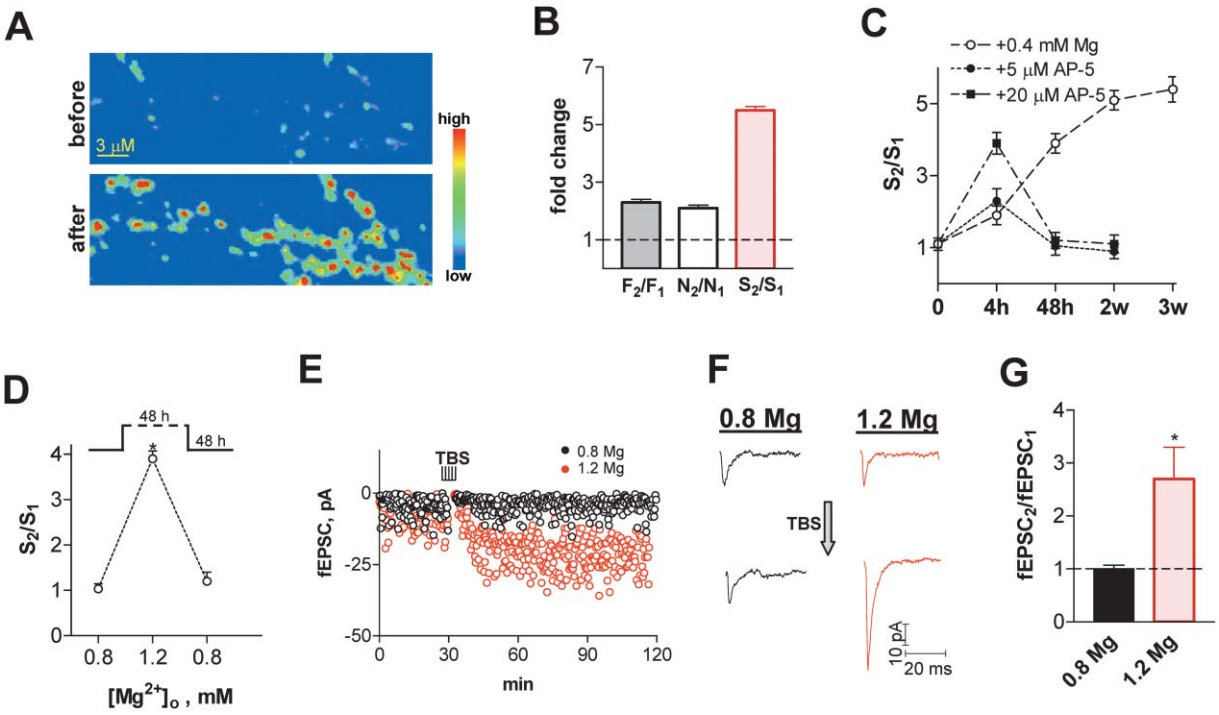

Figure 6. Long-Term Elevation of $[Mg^{2+}]_o$ Enables Synapses to Remain Highly Plastic

(A) Representative fluorescent images before and 30 min after TBS in Mg^{2+}-treated (for 2 weeks) hippocampal culture.

(B) Quantification of changes induced by TBS stimulation: ($\Delta F_2/\Delta F_1 = 2.3 \pm 0.1$ [gray bar], $N_2/N_1 = 2.1 \pm 0.1$ [white bar], $S_2/S_1 = 5.5 \pm 0.2$ [red bar], N = 15).

(C) Time course of enhancement of synaptic plasticity induced by 0.4 mM Mg^{2+} (○), 5 μM AP-5 (●), and 20 μM AP-5 (■).

(D) Mg^{2+}-induced enhancement of plasticity is reversible. Elevation of $[Mg^{2+}]_o$ from 0.8 to 1.2 mM for 48 hr induced the enhancement of synaptic plasticity (the same data as in Figure 6C), and subsequent reduction of $[Mg^{2+}]_o$ back to 0.8 mM for 48 hr returned the terminals to a nonplastic state ($S_2/S_1 = 1.1 \pm 0.2$, N = 3, $p > 0.2$).

(E) The peak amplitude of fEPSC before and after LTP induction by TBS. Black circle, recording from neuron in 0.8 mM $[Mg^{2+}]_o$ cultures; red circle, in 1.2 mM $[Mg^{2+}]_o$ cultures.

(F) Representative traces of EPSC before and 30 min after TBS induction in 0.8 (black traces) and 1.2 (red traces) mM $[Mg^{2+}]_o$ cultures.

(G) Average results of TBS-induced modification of EPSC: $fEPSC_2/fEPSC_1$ is 1.0 ± 0.1 (N = 4) and 2.7 ± 0.6 (N = 5), in 0.8 (black bar) and 1.2 (red bar) mM $[Mg^{2+}]_o$ cultures, respectively.

magnitude of enhancement depended only on the degree of blockade. Complete blockade of NMDA receptor or L-type Ca^{2+} channels induced an ~4-fold enhancement of synaptic plasticity (Figures 4F and 6C). Reduction of NMDAR activity by 50%, whether through application of 5 μM AP-5 or increase of $[Mg]_o$ (0.8 to 1.2 mM), resulted in an ~2-fold enhancement of synaptic plasticity (Figure 6C). On the other hand, for long-term treatments, only the synapses grown under elevated $[Mg]_o$ retain persistent high plasticity. Thus, it was not the scale of the blockade that determined the duration of plasticity enhancement. Rather, it was the blockade's preferential reduction of the Ca^{2+} influx during periods of uncorrelated activity that generated a long-term increase of plasticity.

To test if the Mg^{2+}-induced effect was reversible, the cultures were incubated for 2 days in 1.2 mM $[Mg^{2+}]_o$ and then switched back to control conditions (0.8 mM $[Mg^{2+}]_o$). Exposure to 1.2 mM $[Mg^{2+}]_o$ for 2 days induced a 3.9-fold increase in total presynaptic strength after induction ($n = 2234$, N = 3, $p < 0.001$; Figure 6D). The terminals in higher Mg^{2+} lost their plasticity and returned to control conditions 48 hr after being switched back to 0.8 mM $[Mg^{2+}]_o$ (S_2/S_1 is 1.1 ± 0.2, n = 2739, N = 3, $p >$ 0.2). These data suggest that perturbations in Ca^{2+} flux can reversibly regulate the plasticity of synaptic terminals.

To confirm that such a prominent TBS-induced increase in Pr does contribute to the enhancement of total synaptic strength, the magnitude of potentiation was tested electrophysiologically by sampling field EPSCs (fEPSCs) before and after TBS. The whole-cell recording was obtained under perforated patch configuration to avoid wash out of the intracellular components that are critical for synaptic plasticity. The membrane potential was clamped at −70 mV, and EPSCs were evoked by field stimulation at a sampling frequency of 0.03 Hz. $[Mg^{2+}]_o$ during sampling was 4 mM to reduce background neural activity. The intensity of field stimulation was adjusted to produce a half-maximal fEPSC amplitude. After 30 min of sampling was employed to determine the baseline level of synaptic strength, the bath solution was changed to 1.2 mM $[Mg^{2+}]_o$, and the recording configuration was changed to current-clamp mode to allow for membrane voltage fluctuations. TBS was delivered at the same amplitude and temporal profiles as for the FM experiments. In control cultures (Figures 6E and 6F), as expected, fEPSC size did not change

significantly after TBS (0.9-fold change, $p > 0.2$). In contrast, in the Mg-treated cultures, TBS induced a 2.7-fold increase in fEPSC amplitude ($p < 0.0001$, Figures 6E and 6F). The increase in fEPSC reached a maximum ~10 min after TBS and lasted at least 1.5 hr. On average, no significant change of synaptic strength was found in control cultures (1.0 ± 0.1, N = 4), while synaptic strength increased 2.7-fold (±0.6, N = 5) after TBS induction in the elevated Mg^{2+} treatment cultures (Figure 6G).

Upregulation of NR2B Is an Important Contributor to the Enhancement of Synaptic Plasticity

Our finding that synapses grown under elevated $[Mg^{2+}]_o$ conditions are plastic allows us to identify attributes that determine the plasticity of synapses. The decline of developmental neuronal plasticity mirrors the change of NMDAR subunit composition, particularly a decrease of NR2B-containing receptors (Carmignoto and Vicini, 1992; Sheng et al., 1994). Sensory deprivation, on the other hand, both prolongs ocular dominance plasticity and delays the developmental downregulation of NR2B NMDAR currents (Philpot et al., 2001). In reduced preparations, blockade of neural activity or NMDA currents results in enhanced synaptic localization of NMDARs (Rao and Craig, 1997; Liao et al., 1999). These experimental data suggest that activity-dependent regulation of NMDARs is correlated with modifications in the plasticity of synapses.

Thus, we tested whether the enhancement of synaptic plasticity is associated with an upregulation of NMDAR function. EPSCs were recorded under double-perforated patch configuration (50 μM picrotoxin to block $GABA_A$ channel opening). The membrane potential was held at −70 mV to detect the AMPA component of the evoked response ($EPSC_{-70}$) and at +40 mV for detecting AMPA + NMDA components ($EPSC_{+40}$). $EPSC_{NMDA}$ was then calculated by subtracting a scaled $EPSC_{AMPA}$ from the $EPSC_{+40}$. Figure 7A shows representative EPSCs from neurons cultured under various $[Mg]_o$, showing that the decay of $EPSC_{+40}$ from elevated Mg^{2+}-treated synapses was significantly slower. Further analysis indicated that this was associated with the slower decay of $EPSC_{NMDA}$ (Figure 7B). To get the relative strength of $EPSC_{NMDA}$ over $EPSC_{AMPA}$, we calculated an N/A ratio (defined as G_{NMDA}/G_{AMPA}, G being the integrated conductance of each current). Figure 7C shows that the N/A ratio increased significantly in elevated Mg^{2+} treatment neurons ($p = 0.02$, N = 5 for each condition). From this ratio and the charge transfer of quantal AMPAR-mediated transmission (266 ± 23 fC, N = 6), we calculated the quantal charge transfer through NMDARs (Q_{NMDA}, integrated from t = 0–500 ms). Q_{NMDA} increased by 2.4-fold in neurons cultured with 1.2 mM $[Mg^{2+}]_o$ (Figure 7D). Given the 2-fold change in $EPSC_{NMDA}$ decay, this increase is likely to be entirely due to the prolongation of NMDA currents.

Previous studies have indicated that NMDA current duration is largely controlled by the subunit composition of NMDARs: receptors containing a larger proportion of NR2B subunits exhibit longer currents than those with a larger proportion of NR2A subunits (Flint et al., 1997; Vicini et al., 1998; Tovar et al., 2000). The prolonged decay of $EPSC_{NMDA}$ in the elevated Mg^{2+} treatment neurons might result from an increase in the number of NR2B-containing NMDARs. To test this possibility, we determined the sensitivity of $EPSC_{NMDA}$ to ifenprodil, a selective NR2B blocker, in control versus experimental neurons. Figure 7E shows that, indeed, the ifenprodil sensitivity of $EPSC_{NMDA}$ in elevated Mg^{2+}-treated cultures is much higher than in the controls. On average, in 1.2 mM Mg-treated cultures, an application of 3 μM ifenprodil reduces the total charge transfer by 80% (±4, N = 5, $p < 0.001$). In contrast, in control cultures, the total charge transfer was reduced by only 45% (±2, N = 6, $p < 0.01$, Figure 7F).

These results suggest that, on the postsynaptic side, a reduction in background Ca^{2+} flux induces a 50% increase in NR2B-containing NMDARs and the N/A ratio. To directly evaluate the role of increased NMDAR function in the enhancement of plasticity of presynaptic terminals, we applied the NR2B-selective antagonist ifenprodil (1 μM, current reduced by 53% [N = 3, $p < 0.01$]) to *cancel* the upregulation of NMDAR function induced by the elevation of $[Mg^{2+}]_o$. If the plasticity that we observed was due to changes strictly other than increased NMDAR function, then this perturbation should have had no effect on the enhanced potentiation. However, the magnitude of potentiation was reduced by 50%, suggesting an involvement of NMDAR upregulation in the enhancement of synaptic plasticity (Figure 7G). This data also suggests that other mechanisms are at play. Increased NMDAR function is likely to be an important but not sole factor in the enhancement of synaptic plasticity.

Discussion

Inverse Relationship between the Level of Neural Activity and Plasticity of Synapses

Changes in synaptic activity have been shown to lead to persistent changes in the direction or magnitude of synaptic plasticity, a phenomenon that has been called "metaplasticity" (Abraham and Bear, 1996). Previous studies have shown that even brief periods of several minutes of prior activity can influence the induction threshold of LTP or LTD. In this study, we focused on the long-term relationship between the level of neural activity and the plasticity of synapses. We showed that a reduction in network activity levels resulted in an increase in synaptic plasticity (Figure 4B). While previous work in primary sensory cortices, where plasticity is time delimited by critical periods, has suggested this direction (see Introduction), we have directly established this link for hippocampal neurons, which are known to remain plastic during adult life.

Physiologically, the inverse relationship between neural activity and the plasticity of synapses may be important in the following way: In early phases of the formation of neural circuitry, immature but plastic synapses make weak synaptic connections. Functional strengthening of connections through Hebb-type coincidence detection mechanisms then helps establish computationally meaningful neural connections, leading to elevated overall levels of neural activity within networks. This increase in neural activity may in turn trigger, through the above

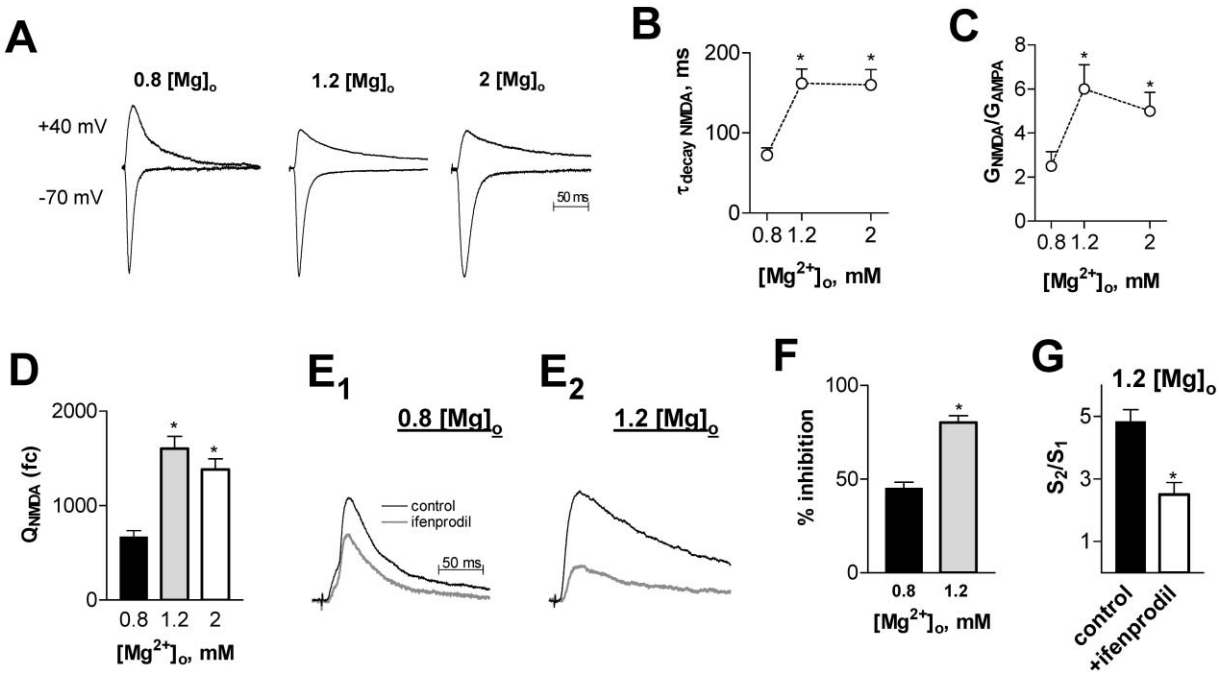

Figure 7. The Long-Term Effects of Elevation of $[Mg^{2+}]_o$ on the $EPSC_{NMDA}$

(A) Recordings of evoked EPSCs at −70 mV and +40 mV (in the presence of 50 μM picrotoxin) between pairs of neurons in control (0.8) and 1.2 and 2 mM Mg^{2+} cultures.

(B) The decay time constant (τ_{decay}) of $EPSC_{NMDA}$ as function of $[Mg^{2+}]_o$.

(C) N/A ratio (calculated as an integral of G_{NMDA}/G_{AMPA}) at different $[Mg^{2+}]_o$.

(D) The charge transfer of quantal $EPSC_{NMDA}$ [$Q_{NMDA\ (-70mV)}$] as a function of $[Mg^{2+}]_o$.

(E) Recordings of $EPSC_{NMDA}$ (in the presence of 1 μM NBQX and 50 μM picrotoxin) in control conditions and after application of 3 μM of ifenprodil in neurons from 0.8 and 1.2 mM Mg^{2+} cultures. The peak amplitudes of EPSC during control recordings were normalized to allow for the comparison of drug sensitivity.

(F) Ifenprodil has stronger inhibitory effects on $EPSC_{NMDA}$ in neurons from 1.2 mM $[Mg^{2+}]_o$ cultures (0.8 mM: 45% ± 2%, N = 6, $p < 0.01$; 1.2 mM: 80% ± 4%, N = 5, $p < 0.001$).

(G) Ifenprodil (1 μM) (IC_{50}) reduced TBS-induced presynaptic potentiation by 48% ± 7% in 1.2 mM Mg^{2+} cultures (N = 4, $p < 0.005$).

mechanism, a reduction in the network's plasticity, which helps "stabilize" those newly strengthened synaptic connections. The reversible nature of this relationship may be essential for the reorganization of in vivo neural circuits when functional inputs are lost. In support of this perspective, deprivation-induced synaptic reorganization is a generic property of adult neocortex. Visual and somatosensory neurons that are silenced by the inactivation of primary inputs can acquire new receptive fields (reviewed in Gilbert et al., 2001). This inverse relationship might facilitate synaptic reorganization mediated through Hebbian-type mechanisms.

Bursting Ca^{2+}, Background Ca^{2+}, and Plasticity

Our data suggest that the plasticity of synaptic terminals is regulated by the quantity (amount) and quality (pattern) of Ca^{2+} flux detected at the postsynaptic spine. In this regard, the enhancement of plasticity in all of our treatments is associated with a reduction of Ca^{2+} flux. However, uniform reductions of Ca^{2+} flux failed to induce long-lasting enhancements of synaptic plasticity, suggesting a complex role for Ca^{2+} flux in the regulation of presynaptic plasticity. The effects of reduction of Ca^{2+} influx on synaptic plasticity can be grouped into two temporal categories:

(1) The response to short-term reduction of Ca^{2+} (~4 hr) is very similar across all treatments. The magnitude of this enhancement of synaptic plasticity is proportional only to the degree of Ca^{2+} flux blockade—the greater the reduction of Ca^{2+} flux, the greater the enhancement. For example, complete blockade of NMDA receptors or L-type Ca^{2+} channels induced an ~4-fold enhancement of synaptic plasticity (Figures 4F and 6C). On the other hand, reduction of NMDA receptor activity by 50% whether through application of 5 μM AP-5 or an increase of $[Mg]_o$ from 0.8 to 1.2 mM resulted in an ~2-fold enhancement of synaptic plasticity (Figure 6C). These similarities suggest a shared mechanism.

(2) However, the response to long-term reduction of Ca^{2+} flux varied by treatment. The enhancement of plasticity lasted only transiently (<24 hr) for uniform reductions of Ca^{2+} flux (AP-5, TTX, flunitrazepam, nimodipine, Figure 4). On the other hand, voltage-dependent reduction of NMDA currents through increased Mg^{2+} block generated a permanent enhancement of synaptic plasticity (Figure 6). This phenomenon suggests that long-term, nonspecific reduction in Ca^{2+} flux might also induce other changes in neural circuits that prevent synapses from staying in a highly potentiable state. One interesting possibility is that the most important difference lies between the levels of Ca^{2+} flux induced by

correlated versus uncorrelated activity. For example, the spatially restricted high levels of Ca^{2+} flux associated with correlated activity can induce potentiation of synaptic connections, while diffuse low levels of Ca^{2+} flux are believed to trigger long-term synaptic depression (Lisman, 1989). It is possible that neural circuitry also distinguishes between these two spatial-temporal patterns in determining long-term properties such as intrinsic synaptic plasticity. The pattern of Ca^{2+} flux in spines could be modified either presynaptically, by altering the frequency-response relationship of transmitter release, or postsynaptically, by perturbing receptors and channels (NMDARs and VGCCs) that translate activity into Ca^{2+} flux. We chose magnesium, the endogenous voltage-dependent pore blocker of NMDARs, to alter the pattern of Ca^{2+} flux. We found that with an increase of $[Mg^{2+}]_o$ within the physiological range (0.8–1.2 mM), the plasticity of synapses was enhanced permanently (>2 weeks, Figure 6).

What synaptic changes induced by higher concentrations of $[Mg^{2+}]_o$ were responsible for the enhancement of the synapse's plasticity? The reduction of background Ca^{2+} influx led to an upregulation of NMDAR function, particularly an increase in the proportion associated with NR2B subunits (Figure 7E). Half-maximal blockade of the NR2B-containing NMDA receptors which restored NMDA currents to their control values led to an inhibition of 50% of TBS-induced plasticity (Figure 7G). This substantial decrease clearly indicates that upregulation of NR2B-containing NMDARs is important in the enhancement of synaptic plasticity. As noted in the Introduction, previous studies in visual and somatosensory cortices have strongly suggested that critical periods of ocular dominance plasticity are matched with changes in NMDAR subunit composition. Mice that were genetically engineered to overexpress NR2B also show increases in hippocampal LTP and learning and memory function (Tang et al., 1999). Due to the substantial increase in NMDA currents (>2-fold) and the accessible nature of our preparation, we are able to directly demonstrate a causal relationship between these two hippocampal processes.

It is important to also note that the reduction of NMDA currents to control levels did *not* eliminate plasticity. This indicates that the upregulation of NR2B-containing NMDARs is not the only relevant regulation point responsible for the enhancement of synaptic plasticity. This finding resonates with recent work in early sensory cortices showing that NR2B subunits and NMDAR currents may play only a limited role in determining their critical periods (Lu et al., 2001; Fagiolini et al., 2003). In addition, we note that NMDA currents increased after short-term blockade of activity and remained elevated after long-term inactivation, even when potentiation was no longer observable (unpublished data). All of this suggests that the functional plasticity of presynaptic terminals is determined by multiple factors—only one of which is postsynaptic NR2-B composition. In this regard, increases in the affinity of the postsynaptic calcium sensor, the amount of BDNF release during TBS (Figure 3), or the sensitivity of presynaptic terminals to the BDNF released may represent other critical regulation points. The ability to turn its plasticity on and off (Figure 6D) and to study its pre- and postsynaptic function separately make our uniquely reduced preparation an inherently attractive option for delineating the roles of the physiological and molecular attributes that determine the plasticity of hippocampal synapses.

Extending the ramifications of this work, it is important to note that Mg^{2+} is also an endogenous trace metal. This raises several questions related to the importance of this mineral in pathological states and putative mechanisms of physiological regulation. Mg^{2+} concentration in healthy human CSF is known to be 1–1.2 mM (Woodbury et al., 1968; Kapaki et al., 1989). Given that our study shows the sensitivity of synaptic plasticity to $[Mg^{2+}]_o$ precisely in this range, we may conclude that maintaining proper $[Mg^{2+}]_o$ in the CSF is essential for maintaining the plasticity of synapses in vivo. Since it is estimated that the majority of American adults consume less than the estimated average requirement of magnesium (Institute of Medicine, 1997), it is possible that such a deficit may have detrimental effects on synaptic plasticity resulting in declines of memory function.

Experimental Procedures

Cell Cultures and Treatments

Hippocampi were dissected from postnatal day 1 rat pups and cultured as previously described (Liu et al., 1999). The experiments were performed in mature (>DIV 15) (Renger et al., 2001) high-density cultures (synaptic density > 1.5 synapses/μm^2 of dendritic surface area). We used a culture medium containing 0.8 mM Mg^{2+} (GIBCO, 51200-038) for control cultures and added various amounts of $MgCl_2$ to raise the Mg^{2+} concentration. For short-term (4–6 hr) and long-term (48 hr) reduction of activity or Ca^{2+} influx, the following drugs were added to the culture medium: 10 μM nimodipine (Tocris), 5 μM flunitrazepam (Sigma), 1 μM NBQX (Sigma), 5 and 20 μM DL-AP5 (Tocris), or 100 nM TTX (Biotium). All experiments involving animals were approved by the Massachusetts Institute of Technology's Committee on Animal Care.

FM Dye Loading and Unloading

Functional presynaptic boutons were stained with 10 μM FM1-43 (synaptogreen, Biotium) by eliciting 30 APs at 0.5–1 Hz. This loading protocol was chosen to avoid short-term plasticity and "re-use" of vesicles through the "kiss-run" mode of exocytosis (Aravanis et al., 2003). The neurons were stimulated to fire action potentials by passing 1 ms 50 mA current through platinum electrodes placed at a distance of 7 mm from both sides of the chamber. To ensure reliable action potential initiation, the current amplitude was chosen to be 50% above the threshold for action potential generation, as confirmed by whole-cell patch clamp recording. To prevent recurrent activity, excitatory postsynaptic responses were blocked completely by the addition of DL-AP-5 (50 μM, Sigma) and NBQX (10 μM, Sigma) during FM loading and unloading procedures. FM dye was present when terminals were stimulated and 30 s after the stimulation (Ryan et al., 1993). For single action potential loading, the duration of dye exposure was reduced to 15 s to minimize nonspecific staining. Following this loading protocol, any external dye that had not been taken up into terminals was washed away in Ca^{2+}-free solution with the addition of quencher ADVASEP-7 (100 μM, Sigma) to speed up dye removal from external membranes (Kay et al., 1999; Zakharenko et al., 2001). Unloading was induced by 2 Hz stimulation for 4 min.

Imaging and Analysis

Imaging was taken using an Olympus (FV300) confocal laser inverted microscope. The 488 nm line of the argon laser was used for excitation, and the emitted light was filtered using a 510 nm long-pass filter and detected by photomultiplier. A 40× 1.15 NA water-immersion objective was used for imaging. For experiments including one AP loading (Figure1, Supplemental Data [http://www.neuron.org/cgi/content/full/44/5/835/DC1/]), images were collected at a resolution

of 1024 × 1024 with a pixel width of 0.11 μm. Confocal aperture was set to maximal. Each image was the average of four images separated by 0.8 μm steps in the z direction. For all other experiments, a confocal aperture was partially open and image resolution was reduced to 0.138 μm/pixel. The gain of the photomultiplier was adjusted to maximize the signal/noise ratio without causing saturation by the strongest signals. The image after FM dye unloading was subtracted from the initial image; thus, only those terminals containing activity-dependent releasable FM dye (~90% of total staining) were analyzed. FM-positive puncta were selected for further analysis using custom scripts written in ImagePro Plus (Media Cybernetics, Carlsbad, CA) and MATLAB (Mathworks, Natick, MA) programs, based on following criteria: the fluorescence intensity (ΔF) was 3 standard deviations above the mean background and the diameter of spots was between 0.1 and 0.6 μm.

Retrospective Immunohistochemistry

Following functional FM1-43 staining, neurons were fixed by flooding the perfusion chamber with a fixative FSB solution consisting of 4% paraformaldehyde and 4% sucrose in 1x PBS for 30 min and permeabilized with 0.5% Triton X-100. Primary antibodies against VGLUT1 (Chemicon International), and GAD65 (Chemicon International) were applied for 8 hr, followed by rinses in PBS and staining with Alexa 488- and 633-conjugated secondary antibodies (1/400; Molecular Probes, Eugene, OR) at 22°C–24°C. All images were collected at 1024 × 1024 pixels with a 0.069 μm/pixel resolution. Eleven images separated by 0.8 μm steps in the z direction were compressed to generate the final image. Images of the fixed and immunolabeled tissue were aligned with corresponding FM images of the same region.

Electrophysiology

Dual whole-cell perforated patch clamp recordings were made on two interconnected cultured hippocampal pyramidal neurons. Perforated patch pipettes were front filled with a solution containing CsOH, 127 mM; D-gluconic acid, 127 mM; CsCl, 4 mM; HEPES, 10 mM; NaCl, 8 mM; and EGTA, 0.4 mM; pH was adjusted to 7.25 with CsOH and then back filled with the same solution containing 150–220 ng/ml amphotericin B (Sigma, St. Louis, MO). Extracellular solution contained NaCl, 145 mM; KCl, 3 mM; glucose, 15 mM; HEPES, 10 mM; $MgCl_2$, 0.8–1.2 mM; $CaCl_2$, 1.2 mM; glycine, 0.005 mM (Sigma); and picrotoxin, 0.05 mM (Sigma); pH adjusted to 7.4 with NaOH. $MgCl_2$ concentration was matched to its concentration in culture medium. In experiments where effects of drugs on neuronal activity were quantified (Figure 4D), recordings were done in culture medium (with HEPES replacing bicarbonate/CO_2 to maintain pH). All experiments were performed at room temperature. For assaying synaptic connectivity, each neuron was stimulated by 1 ms step depolarization from −70 to +30 mV in voltage-clamp mode. Only neurons with monosynaptic connections were used. The access resistances of both pre- and postsynaptic neurons were monitored online and were typically 7–20 MΩ. Recordings with access resistance > 20 MΩ or that varied substantially were rejected from analysis.

For studying the voltage dependence of NMDAR Mg^{2+} block (Figure 5), NMDA currents were evoked by local application of glutamate using the high-speed iontophoresis technique (Murnick et al., 2002). The current traces for each cell were normalized to their value at +40 mV membrane potential. The voltage dependency of NMDA currents was modeled using the Woodhull function (Woodhull, 1973). The NMDA channel conductance in the presence and absence of Mg^{2+} was related according to the relationship:

$$\frac{g}{g_{max}} = \frac{1}{1 + \frac{[Mg^{++}]_o}{K_{Mg}} e^{\left(-\frac{z\delta EF}{RT}\right)}} \quad (1)$$

where K_{Mg} is the voltage-independent affinity of Mg^{2+} for the channel (0 mV membrane potential), δ is the electrical distance of the Mg^{2+} binding site in the membrane field, E is membrane potential, and z is the valence of the blocking ion. RT/F was 25.4 mV (21°C).

Calcium Imaging

An Olympus (FV300) confocal laser-scanning system was used to perform calcium and structural imaging. The single wavelength calcium indicator Fluo-5F (K_d ~1.6 μM, Molecular Probes) was loaded into the neuron under a whole-cell patch clamping configuration. The intracellular pipette solution contained 130 mM $CsMeSO_3$, 10 mM HEPES, 10 mM sodium phosphocreatine, 4 mM $MgCl_2$, 4 mM Na_2-ATP, 0.4 mM Na_2-GTP, and 0.02 mM Alexa Fluor-633 (Molecular Probes); pH was adjusted to 7.25. The pipette resistance ranged from 2 to 3 MΩ, and calcium imaging was performed at room temperature. For most experiments, images were taken 30–40 min after establishing whole-cell recording to allow equilibration of indicators in spines located 50–150 μm from the cell body (where the actual measurements were performed). NMDA receptors at single spines were activated by local application of glutamate using high-speed iontophoresis every 20 s. Fluo-5F and Alexa Fluor-633 were excited with two different wavelengths, 488 and 633 nm, by argon and helium lasers, respectively. Imaging with Alexa Fluor-633 fluorescence was used to visualize dendritic morphology. To avoid photodynamic damage of the cell, the laser intensity was set to 0.1% (of 5 and 25 mW, respectively). This allowed us to obtain stable Ca^{2+} images over at least 1 hr. To measure the temporal profile of $[Ca^{2+}]$ changes at the spine head, we used the line-scanning mode (500 Hz, Figures 5E and 5F). Baseline fluorescence (F_0) was measured for 50 ms prior to the stimulus, and ΔF/F was calculated as $(\Delta F/F)_t = (F_t - F_0)/F_0$. We periodically monitored AP-evoked $[Ca^{2+}]$ transients as an index of dendritic viability. Data analysis was performed using ImagePro Plus (Media Cybernetics, Carlsbad, CA).

Statistical Analysis

Error bars shown represent the standard error of the mean (SEM). Statistical significance was considered to be $p < 0.05$ and is indicated in the figures by an asterisk. For each experimental condition that contributed to the analysis, N represents the number of separate cultures used, and n represents the total number of individual synapses. Means were compared with the Student's t test.

Acknowledgments

This work was supported by the RIKEN-MIT Neuroscience Center and National Institutes of Health grants NS37342 and MH58880. We are grateful to Matt Wilson and Mark Bear for their careful reading of the manuscript and helpful comments. We thank Travis Emery for his superb assistance. We also thank Regeneron for TrkB-IgG.

In memoriam: To our editor, Dr. Anuradha Rao, whose insight and warmth shone on us and our work alike.

Received: February 18, 2004
Revised: July 27, 2004
Accepted: November 8, 2004
Published: December 1, 2004

References

Abraham, W.C., and Bear, M.F. (1996). Metaplasticity: the plasticity of synaptic plasticity. Trends Neurosci. *19*, 126–130.

Allen, C., and Stevens, C.F. (1994). An evaluation of causes for unreliability of synaptic transmission. Proc. Natl. Acad. Sci. USA *91*, 10380–10383.

Aravanis, A.M., Pyle, J.L., and Tsien, R.W. (2003). Single synaptic vesicles fusing transiently and successively without loss of identity. Nature *423*, 643–647.

Bacci, A., Coco, S., Pravettoni, E., Schenk, U., Armano, S., Frassoni, C., Verderio, C., De Camilli, P., and Matteoli, M. (2001). Chronic blockade of glutamate receptors enhances presynaptic release and downregulates the interaction between synaptophysin-synaptobrevin-vesicle-associated membrane protein 2. J. Neurosci. *21*, 6588–6596.

Bear, M.F. (2003). Bidirectional synaptic plasticity: from theory to reality. Philos. Trans. R. Soc. Lond. B Biol. Sci. *358*, 649–655.

Betz, W.J., Mao, F., and Bewick, G.S. (1992). Activity-dependent

fluorescent staining and destaining of living vertebrate motor nerve terminals. J. Neurosci. *12*, 363–375.

Bi, G.Q., and Poo, M.M. (1998). Synaptic modifications in cultured hippocampal neurons: dependence on spike timing, synaptic strength, and postsynaptic cell type. J. Neurosci. *18*, 10464–10472.

Bliss, T.V., and Collingridge, G.L. (1993). A synaptic model of memory: long-term potentiation in the hippocampus. Nature *361*, 31–39.

Boulanger, L., and Poo, M.M. (1999). Presynaptic depolarization facilitates neurotrophin-induced synaptic potentiation. Nat. Neurosci. *2*, 346–351.

Buonomano, D.V., and Merzenich, M.M. (1998). Cortical plasticity: from synapses to maps. Annu. Rev. Neurosci. *21*, 149–186.

Carmignoto, G., and Vicini, S. (1992). Activity-dependent decrease in NMDA receptor responses during development of the visual cortex. Science *258*, 1007–1011.

Chang, E.F., and Merzenich, M.M. (2003). Environmental noise retards auditory cortical development. Science *300*, 498–502.

Chutkow, J.G. (1974). Metabolism of magnesium in central nervous system. Relationship between concentrations of magnesium in cerebrospinal fluid and brain in magnesium deficiency. Neurology *24*, 780–787.

Fagiolini, M., Pizzorusso, T., Berardi, N., Domenici, L., and Maffei, L. (1994). Functional postnatal development of the rat primary visual cortex and the role of visual experience: dark rearing and monocular deprivation. Vision Res. *34*, 709–720.

Fagiolini, M., Katagiri, H., Miyamoto, H., Mori, H., Grant, S.G., Mishina, M., and Hensch, T.K. (2003). Separable features of visual cortical plasticity revealed by N-methyl-D-aspartate receptor 2A signaling. Proc. Natl. Acad. Sci. USA *100*, 2854–2859.

Flint, A.C., Maisch, U.S., Weishaupt, J.H., Kriegstein, A.R., and Monyer, H. (1997). NR2A subunit expression shortens NMDA receptor synaptic currents in developing neocortex. J. Neurosci. *17*, 2469–2476.

Fox, K. (1992). A critical period for experience-dependent synaptic plasticity in rat barrel cortex. J. Neurosci. *12*, 1826–1838.

Gilbert, C.D., Sigman, M., and Crist, R.E. (2001). The neural basis of perceptual learning. Neuron *31*, 681–697.

Institute of Medicine. (1997). Dietary Reference Intakes of Calcium, Phosphorus, Magnesium, Vitamin D, and Fluoride (Washington, D.C.: National Academic Press).

Jahr, C.E., and Stevens, C.F. (1990). A quantitative description of NMDA receptor-channel kinetic behavior. J. Neurosci. *10*, 1830–1837.

Jahr, C.E., and Stevens, C.F. (1993). Calcium permeability of the N-methyl-D-aspartate receptor channel in hippocampal neurons in culture. Proc. Natl. Acad. Sci. USA *90*, 11573–11577.

Kang, H., Welcher, A.A., Shelton, D., and Schuman, E.M. (1997). Neurotrophins and time: different roles for TrkB signaling in hippocampal long-term potentiation. Neuron *19*, 653–664.

Kapaki, E., Segditsa, J., and Papageorgiou, C. (1989). Zinc, copper and magnesium concentration in serum and CSF of patients with neurological disorders. Acta Neurol. Scand. *79*, 373–378.

Katz, L.C., and Shatz, C.J. (1996). Synaptic activity and the construction of cortical circuits. Science *274*, 1133–1138.

Kay, A.R., Alfonso, A., Alford, S., Cline, H.T., Holgado, A.M., Sakmann, B., Snitsarev, V.A., Stricker, T.P., Takahashi, M., and Wu, L.G. (1999). Imaging synaptic activity in intact brain and slices with FM1-43 in *C. elegans*, lamprey, and rat. Neuron *24*, 809–817.

Kovalchuk, Y., Eilers, J., Lisman, J., and Konnerth, A. (2000). NMDA receptor-mediated subthreshold Ca(2+) signals in spines of hippocampal neurons. J. Neurosci. *20*, 1791–1799.

Li, Y.X., Zhang, Y., Lester, H.A., Schuman, E.M., and Davidson, N. (1998). Enhancement of neurotransmitter release induced by brain-derived neurotrophic factor in cultured hippocampal neurons. J. Neurosci. *18*, 10231–10240.

Liao, D., Zhang, X., O'Brien, R., Ehlers, M.D., and Huganir, R.L. (1999). Regulation of morphological postsynaptic silent synapses in developing hippocampal neurons. Nat. Neurosci. *2*, 37–43.

Lisman, J. (1989). A mechanism for the Hebb and the anti-Hebb processes underlying learning and memory. Proc. Natl. Acad. Sci. USA *86*, 9574–9578.

Lisman, J.E. (1997). Bursts as a unit of neural information: making unreliable synapses reliable. Trends Neurosci. *20*, 38–43.

Liu, G. (2004). Local structural balance and functional interaction of excitatory and inhibitory synapses in hippocampal dendrites. Nat. Neurosci. *7*, 373–379.

Liu, G., Choi, S., and Tsien, R.W. (1999). Variability of neurotransmitter concentration and nonsaturation of postsynaptic AMPA receptors at synapses in hippocampal cultures and slices. Neuron *22*, 395–409.

Lu, B. (2003). BDNF and activity-dependent synaptic modulation. Learn. Mem. *10*, 86–98.

Lu, H.C., Gonzalez, E., and Crair, M.C. (2001). Barrel cortex critical period plasticity is independent of changes in NMDA receptor subunit composition. Neuron *32*, 619–634.

Mackenzie, P.J., Umemiya, M., and Murphy, T.H. (1996). Ca^{2+} imaging of CNS axons in culture indicates reliable coupling between single action potentials and distal functional release sites. Neuron *16*, 783–795.

Mayer, M.L., and Westbrook, G.L. (1987). Permeation and block of N-methyl-D-aspartic acid receptor channels by divalent cations in mouse cultured central neurones. J. Physiol. *394*, 501–527.

Mayer, M.L., Westbrook, G.L., and Guthrie, P.B. (1984). Voltage-dependent block by Mg2+ of NMDA responses in spinal cord neurones. Nature *309*, 261–263.

Murnick, J.G., Dube, G., Krupa, B., and Liu, G. (2002). High-resolution iontophoresis for single-synapse stimulation. J. Neurosci. Methods *116*, 65–75.

Murthy, V.N., and Stevens, C.F. (1998). Synaptic vesicles retain their identity through the endocytic cycle. Nature *392*, 497–501.

Murthy, V.N., Sejnowski, T.J., and Stevens, C.F. (1997). Heterogeneous release properties of visualized individual hippocampal synapses. Neuron *18*, 599–612.

Murthy, V.N., Schikorski, T., Stevens, C.F., and Zhu, Y. (2001). Inactivity produces increases in neurotransmitter release and synapse size. Neuron *32*, 673–682.

Nowak, L., Bregestovski, P., Ascher, P., Herbet, A., and Prochiantz, A. (1984). Magnesium gates glutamate-activated channels in mouse central neurones. Nature *307*, 462–465.

Philpot, B.D., Sekhar, A.K., Shouval, H.Z., and Bear, M.F. (2001). Visual experience and deprivation bidirectionally modify the composition and function of NMDA receptors in visual cortex. Neuron *29*, 157–169.

Raastad, M., and Shepherd, G.M. (2003). Single-axon action potentials in the rat hippocampal cortex. J. Physiol. *548*, 745–752.

Rao, A., and Craig, A.M. (1997). Activity regulates the synaptic localization of the NMDA receptor in hippocampal neurons. Neuron *19*, 801–812.

Renger, J.J., Egles, C., and Liu, G. (2001). A developmental switch in neurotransmitter flux enhances synaptic efficacy by affecting AMPA receptor activation. Neuron *29*, 469–484.

Ryan, T.A., and Smith, S.J. (1995). Vesicle pool mobilization during action potential firing at hippocampal synapses. Neuron *14*, 983–989.

Ryan, T.A., Reuter, H., Wendland, B., Schweizer, F.E., Tsien, R.W., and Smith, S.J. (1993). The kinetics of synaptic vesicle recycling measured at single presynaptic boutons. Neuron *11*, 713–724.

Ryan, T.A., Smith, S.J., and Reuter, H. (1996). The timing of synaptic vesicle endocytosis. Proc. Natl. Acad. Sci. USA *93*, 5567–5571.

Sabatini, B.L., Oertner, T.G., and Svoboda, K. (2002). The life cycle of Ca(2+) ions in dendritic spines. Neuron *33*, 439–452.

Schikorski, T., and Stevens, C.F. (2001). Morphological correlates of functionally defined synaptic vesicle populations. Nat. Neurosci. *4*, 391–395.

Shatz, C.J., and Stryker, M.P. (1988). Prenatal tetrodotoxin infusion

blocks segregation of retinogeniculate afferents. Science *242*, 87–89.

Shelton, D.L., Sutherland, J., Gripp, J., Camerato, T., Armanini, M.P., Phillips, H.S., Carroll, K., Spencer, S.D., and Levinson, A.D. (1995). Human trks: molecular cloning, tissue distribution, and expression of extracellular domain immunoadhesins. J. Neurosci. *15*, 477–491.

Sheng, M., Cummings, J., Roldan, L.A., Jan, Y.N., and Jan, L.Y. (1994). Changing subunit composition of heteromeric NMDA receptors during development of rat cortex. Nature *368*, 144–147.

Stryker, M.P., and Harris, W.A. (1986). Binocular impulse blockade prevents the formation of ocular dominance columns in cat visual cortex. J. Neurosci. *6*, 2117–2133.

Tang, Y.P., Shimizu, E., Dube, G.R., Rampon, C., Kerchner, G.A., Zhuo, M., Liu, G., and Tsien, J.Z. (1999). Genetic enhancement of learning and memory in mice. Nature *401*, 63–69.

Thiagarajan, T.C., Piedras-Renteria, E.S., and Tsien, R.W. (2002). alpha- and betaCaMKII. Inverse regulation by neuronal activity and opposing effects on synaptic strength. Neuron *36*, 1103–1114.

Timney, B., Mitchell, D.E., and Giffin, F. (1978). The development of vision in cats after extended periods of dark-rearing. Exp. Brain Res. *31*, 547–560.

Tovar, K.R., Sprouffske, K., and Westbrook, G.L. (2000). Fast NMDA receptor-mediated synaptic currents in neurons from mice lacking the epsilon2 (NR2B) subunit. J. Neurophysiol. *83*, 616–620.

Turrigiano, G.G., and Nelson, S.B. (2004). Homeostatic plasticity in the developing nervous system. Nat. Rev. Neurosci. *5*, 97–107.

Vicini, S., Wang, J.F., Li, J.H., Zhu, W.J., Wang, Y.H., Luo, J.H., Wolfe, B.B., and Grayson, D.R. (1998). Functional and pharmacological differences between recombinant N-methyl-D-aspartate receptors. J. Neurophysiol. *79*, 555–566.

Wiesel, T.N., and Hubel, D.H. (1963). Single-cell responses in striate cortex of kittens deprived of vision in one eye. J. Neurophysiol. *26*, 1003–1017.

Woodbury, J., Lyons, K., Carretta, R., Hahn, A., and Sullivan, J.F. (1968). Cerebrospinal fluid and serum levels of magnesium, zinc, and calcium in man. Neurology *18*, 700–705.

Woodhull, A.M. (1973). Ionic blockage of sodium channels in nerve. J. Gen. Physiol. *61*, 687–708.

Yuste, R., and Denk, W. (1995). Dendritic spines as basic functional units of neuronal integration. Nature *375*, 682–684.

Zakharenko, S.S., Zablow, L., and Siegelbaum, S.A. (2001). Visualization of changes in presynaptic function during long-term synaptic plasticity. Nat. Neurosci. *4*, 711–717.

Zakharenko, S.S., Patterson, S.L., Dragatsis, I., Zeitlin, S.O., Siegelbaum, S.A., Kandel, E.R., and Morozov, A. (2003). Presynaptic BDNF required for a presynaptic but not postsynaptic component of LTP at hippocampal CA1–CA3 synapses. Neuron *39*, 975–990.